Cosmic ray composition estimation below the knee of the spectrum from the time structure of Čerenkov light in EAS

M.D. Roberts

Institute for Cosmic Ray Research, University of Tokyo, Tokyo 188-8502, Japan

Monte Carlo simulations show that the pulse profile of Čerenkov photons measured near the core of an extensive air shower is sensitive to the secondary muon/electron ratio of the cascade. Čerenkov pulses can easily be measured with a single large area mirror viewed by a photomultiplier tube subtending a small field of view ($\sim 1^{\circ}$). Even for such a simple experiment, exposed to EAS from a range of core locations and arrival directions, strong statistical differences are shown to exist between the pulse parameter distributions of primary protons and those of heavier primary particles. A range of primary energies can be investigated by varying the zenith angle of observations. In this paper, results from simulations of primaries in the energy range 20 TeV to 400 TeV are presented, although in principle the technique could be extended to include the knee of the spectrum. At the lower end of this energy range results can be compared to direct measurements of the composition, while measurements at the upper end can augment results from existing ground based experiments.

1 Introduction

The chemical composition of cosmic rays measured at the Earth is an important key to understanding the production and propagation of cosmic rays. Up to $\sim$ 1TeV per particle the flux of cosmic rays is sufficiently high that direct measurements of high statistical significance can be made with satellite or balloon based detectors. At energies of 100TeV per particle the flux of primaries is so low that direct composition measurements are limited by large statistical uncertainties. Current knowledge of the composition at 100TeV, obtained from direct measurement, is summarized in [11].

Above 100TeV primary fluxes are such that cosmic rays can only be studied through extensive air showers (EAS), generated as the primaries interact with

the earth's atmosphere. At ground level EAS can be characterized by measuring secondary electrons, muons, hadrons and Čerenkov light. If the primary energy is sufficiently large ($> 10^{17}$eV) fluorescence light from nitrogen excitation is also detectable. On average, EAS from primaries of different mass will develop in different ways, leading to composition dependent differences in the secondary observables. In practice, inherent fluctuations in the development of EAS and the complexity of interpreting ground level measurements has limited the success of composition measurement around the knee of the spectrum ($\sim 10^{15}$eV). Historically, the mass resolution of ground based experiments has been so poor that results are expressed as the ratio of light (protons and helium) to heavy (mass > helium) components. Estimates of this ratio at the knee from current experiments vary considerably ($\sim$0.3 to $\sim$0.6 [11]) although there is general agreement that the average composition around the knee becomes heavier with increasing energy. Several new experiments, designed to simultaneously measure many of the secondary observables of EAS, should improve considerably the current knowledge of the cosmic ray composition around the knee of the spectrum [2,5,7,8].

2 Čerenkov light from extensive air showers

The arrival time distribution of Čerenkov photons from EAS has been studied for a large range of primary particle energies (see, for example [3,1] and references therein). For vertically incident primaries with energy >100TeV, which are detectable by ground level particle arrays, the vast majority of Čerenkov photons come from the electromagnetic (EM) component of the cascade. In this case the basic core-distance dependent time structure of the Čerenkov pulse can be described by the simple model outlined in [4]. Most of the Čerenkov emission occurs from energetic particles traveling at speed c near the core of the shower, which can be approximated as a single line of emission. The time structure is determined by a combination of varying distances and refractive index induced delays between the observer and different parts of the cascade. At the core, photons from the bottom of the shower will arrive first, with photons emitted higher up being delayed by the refractive index of the atmosphere. Away from the core the Čerenkov photons emitted at the bottom of the cascade experience greater geometrical delays than those emitted higher up. At the "Čerenkov shoulder"([9]) refractive and geometrical delays cancel and , in this simple model, photons from all parts of the cascade arrive simultaneously. Beyond the Čerenkov shoulder the geometrical delays dominate and the width of the pulse becomes a strong function of core distance. Clearly the greater the longitudinal extent of the shower, the wider the Čerenkov pulse at most core locations.

The simple model described above predicts reasonably well the general behav-

ior of Čerenkov pulses from EAS. For real cascades, however, the relationship between core location and Čerenkov pulse width is blurred by the distribution of particle energies and the finite lateral extent of the shower core. The model also ignores the contribution of Čerenkov light from muons.

The highest energy muons are created early in the hadronic core of the cascade and can easily survive to produce Čerenkov light down to ground level. This light will arrive in advance of light produced by the EM component of the cascade. The total muon energy of the cascade is carried by relatively few particles leading to a poor efficiency in Čerenkov production compared to the EM component. As the energy of the primary is reduced, however, the relative contribution of the muons to the total Čerenkov yield is increased. This is particularly true for the region inside the shoulder of the lateral distribution, where many of the photons from the the most deeply penetrating part of the EM cascade arrive ([9]). As the primary energy increases, the multiplicative nature of the EM cascade efficiently converts the extra primary energy into large numbers of Čerenkov producing electrons. The cascade develops deeper in the atmosphere, so the Čerenkov light is more concentrated at ground level and suffers less atmospheric absorption than light produced higher in the atmosphere. While a higher energy primary also results in more energy in the muon channel, much of that energy is carried by a few very energetic muons or partly lost to the EM component if the charged pions interact rather than decay.

For a vertically incident primary hadron of a few TeV, the simple model of Čerenkov pulse production described previously becomes inadequate. The electromagnetic component of the cascade will develop rapidly, and within $\sim$150m of the core the Čerenkov light produced will appear as a "flash" inasmuch as the duration will be short compared to the duration of the entire pulse. The majority of the time structure of the pulse comes from Čerenkov light from penetrating muons that appears on the leading edge of the pulse. The ratio of light on the leading edge to that in the "flash" will reflect the ratio of muons/electrons in the cascade capable of generating Čerenkov light.

The total time spread of Čerenkov photons observed within the shoulder of the lateral distribution is determined by the atmospheric thickness between the EM Čerenkov emission and the observer. If observations are made at sufficiently large zenith angles, the timing separation between EM and muonic Čerenkov light will be maintained for even a very energetic primary.

3 The dependence of the pulse profile on the mass of the primary

The effect of primary mass on the shape of the Čerenkov pulse profile can be predicted through general arguments about EAS development: a detailed characterization of pulse profiles, obtained from Monte Carlo simulations, will be presented in section 5. Assuming maximal or near-maximal fragmentation of the primary nuclei, consider now the differences in the development of the electromagnetic components of EAS generated by protons and iron nuclei of the same total energy. The longitudinal development profiles of proton and iron induced EAS are remarkably similar ([7]). The individual sub-showers from the nucleons of the iron primary develop and decay more rapidly than the primary proton EAS, but these component nucleons interact at a variety of atmospheric depths effectively elongating the cascade. While the development of the proton and iron cascades will have similar profiles, on average the iron cascades will develop higher in the atmosphere. The transverse momentum of the pions in a cascade increases only slowly with total momentum ([12]), so the lateral extent of the secondary particles in the iron cascade will be greater than that of the proton cascade. The combination of these two effects - height of maximum and wider lateral distribution, result in the Čerenkov light from the EM component of the iron induced EAS being more diffuse at ground level than for the proton induced EAS. Over the energy range considered here, the Čerenkov photon density at ground level for a primary iron nucleus is about half that of a primary proton of the same total energy.

The arguments used to describe the development of the EM cascade also apply to some extent to the muonic component of the cascade: the muons in the iron cascade tend to be produced higher and with greater lateral spread. The muonic cascade from the iron primary is , however, much more efficient at producing Čerenkov light. The energy of the muonic component of an iron induced cascade is carried by large numbers of relatively low energy muons. The much higher energy interactions at the hadronic core of the proton cascade provides fewer muons with larger average energy. The overall result is that the ratio of the total Čerenkov light that is derived from the muons increases with increasing primary mass.

4 Measuring Čerenkov pulse profiles

To fully exploit the mass dependent differences between EAS, the detector must be able to collect enough photons to make a detailed pulse profile for those EAS with EM components maximizing high in the atmosphere. The bandwidth of the system must be high, and the field of view sufficiently small that pulse parameterization is not seriously affected by the night sky back-

ground. An isochronous large area mirror, such as those used in TeV gamma-ray astronomy, viewed by a single photomultiplier tube would fulfill these conditions. The use of such a system for cosmic ray composition measurement has been described in [10], and examined in detail for VHE cosmic rays (E<10TeV) in [1].

At any single zenith angle the range of primary energies that can be investigated is quite limited. The primary energy must be sufficiently high that a large number of Čerenkov photons are available but the steep nature of the primary energy spectrum and the shape of the Čerenkov lateral distribution bias any sample towards lower energy events. The higher the primary energy at a fixed zenith angle the less distinct is the timing separation between the Čerenkov light of muonic and EM origin (see section 2). A further consideration is that for the higher energy events, the apparent image size is much larger so that on average less of the total angular distribution of the Čerenkov light is sampled by a narrow FOV detector.

Fortunately the limited energy range is easily overcome by observing at a range of zenith angles. The total atmospheric thickness changes from $\sim$1000 gcm^{-2} at zenith to $\sim$36000 gcm^{-2} for horizontal observations. This, in principal, would allow Čerenkov composition measurements over a very large energy range (a few TeV to tens of PeV). Observing at large zenith angles provides increased collection area for the higher energy primaries, and also provides a greater distance over which the Čerenkov emission can occur. This tends to stretch the pulse out, making the timing measurement easier and less affected by systematic uncertainties in the measurement system.

A system similar to that described above has been operated on the BIGRAT atmospheric Čerenkov detector. This system comprised a 4m diameter parabolic mirror viewed by a single photomultiplier tube subtending a field of view (FOV) of $\sim 1.0^{\circ}$. The system was designed to be sensitive to the differences between Čerenkov pulses initiated by gamma-rays and cosmic rays for large zenith angle observations. While no detailed composition analysis was performed, it was noted that the shape of the cosmic ray pulse profiles was inconsistent with a pure proton composition ([10]).

5 Monte Carlo Simulations

The Monte Carlo simulations presented here have been made using CORSIKA version 4.5 [6], with GHEISHA code for low energy hadrons and VENUS for high energy hadrons. The EM cascade is fully simulated using the EGS routines and Rayleigh, Mie and ozone absorption processes are modeled for the Čerenkov light. The detector consists of a single 5m diameter isochronous

Table 1
Summary of the Monte Carlo simulation data set. The maximum arrival direction for all primaries is limited to 2.0° from the center of the field of view.

primary	zenith	minimum energy (TeV)	maximum core distance (m)
proton	60°	15	450
helium	60°	20	450
oxygen	60°	20	450
iron	60°	30	450
proton	70°	100	720
iron	70°	200	720

light collector located at 160m above sea level. The mirror is viewed by a single photomultiplier tube with assumed bialkali spectral sensitivity, subtending a full FOV of 1.6°. This FOV has not been rigorously optimized for pulse profile measurement: it is large enough that it can sample most of the angular distribution of the EAS of interest, and small enough to exclude very large-arrival-angle large-core-distance cascades. The photoelectrons detected by the photomultiplier are converted into a pulse by convolving the arrival time of each photoelectron with a simple symmetric detector response function with a rise-time (0-100%) of 2ns. The waveform that is generated is sampled 4 times per nano-second. The night sky background is simulated by adding Poisson distributed photoelectrons to the waveform at an average rate of 2 per nano-second.

In this paper, results of simulations at 60° and 70° from zenith will be presented. At 60° proton, helium, oxygen and iron primaries have been simulated, but only proton and iron at 70° from zenith. To model a single telescope realistically it is important to include primaries over the full range of energies, core locations and arrival directions to which the instrument is sensitive (see table 1 for a summary). For all species an integral spectral index of -1.6 has been assumed. To reduce computing time each shower has been sampled a total of eight times.

At 60° and 70° from zenith the slant distances are ~ 2 and ~ 3 vertical atmospheres respectively. It is possible to extend the energy range of observations up to the knee region by observing at even larger zenith angles, but this is beyond the limitations of the Monte Carlo simulation package used here. CORSIKA v4.5 uses a flat earth/atmosphere and beyond $\sim 70°$ this leads to increasing inaccuracies in describing the depth profile of the atmosphere. At extreme zenith angles the atmospheric depth also changes considerably across the full angular acceptance of the detector ($\sim 4°$), further complicating

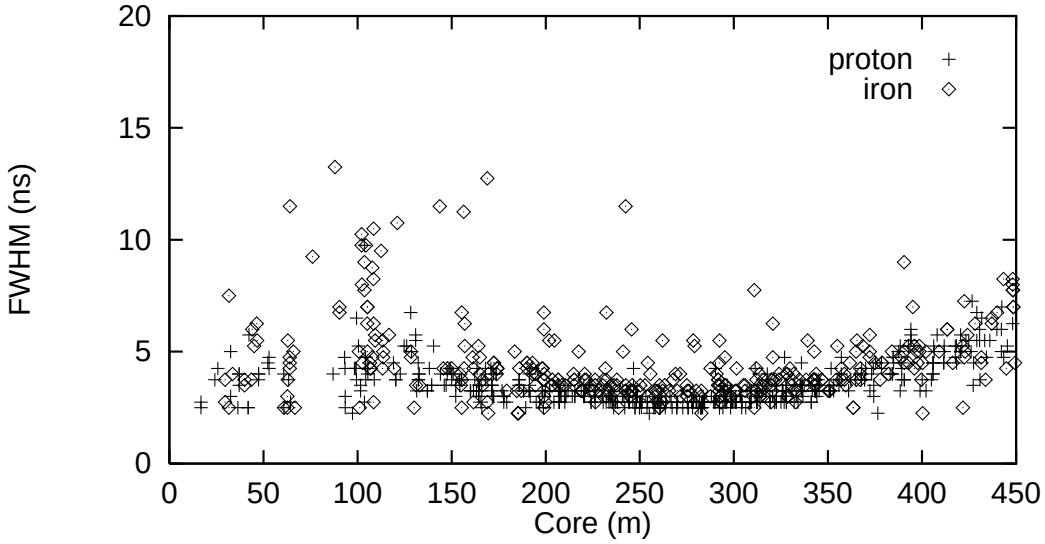

Fig. 1. FWHM of the Čerenkov light pulse versus core location for primary proton and iron induced EAS at 60° from zenith . The pulses contain between 600 and 900 photoelectrons (Monte Carlo simulation)

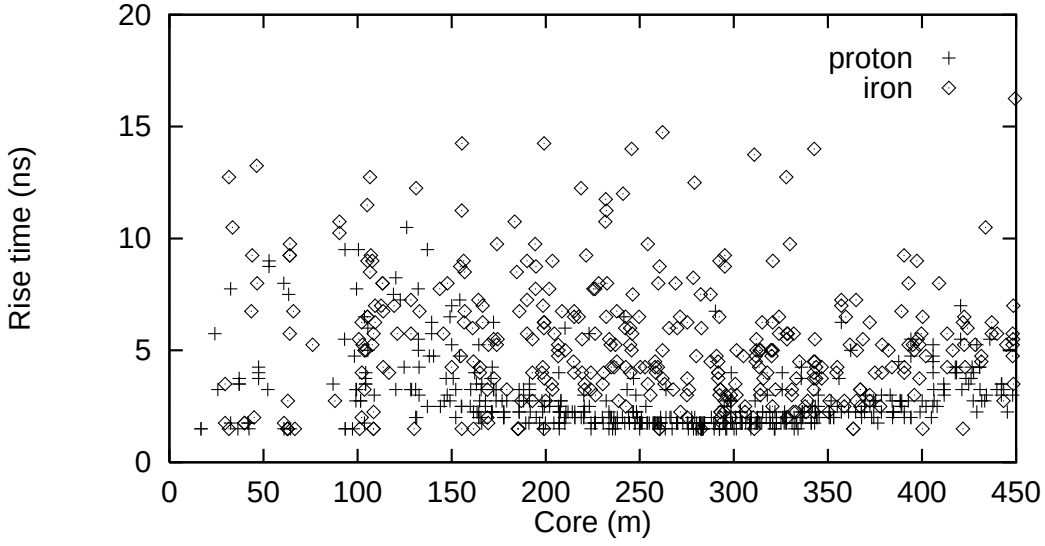

Fig. 2. Rise-time of the Čerenkov light pulse versus core location for primary proton and iron induced EAS at 60° from zenith . The pulses contain between 600 and 900 photoelectrons (Monte Carlo simulation)

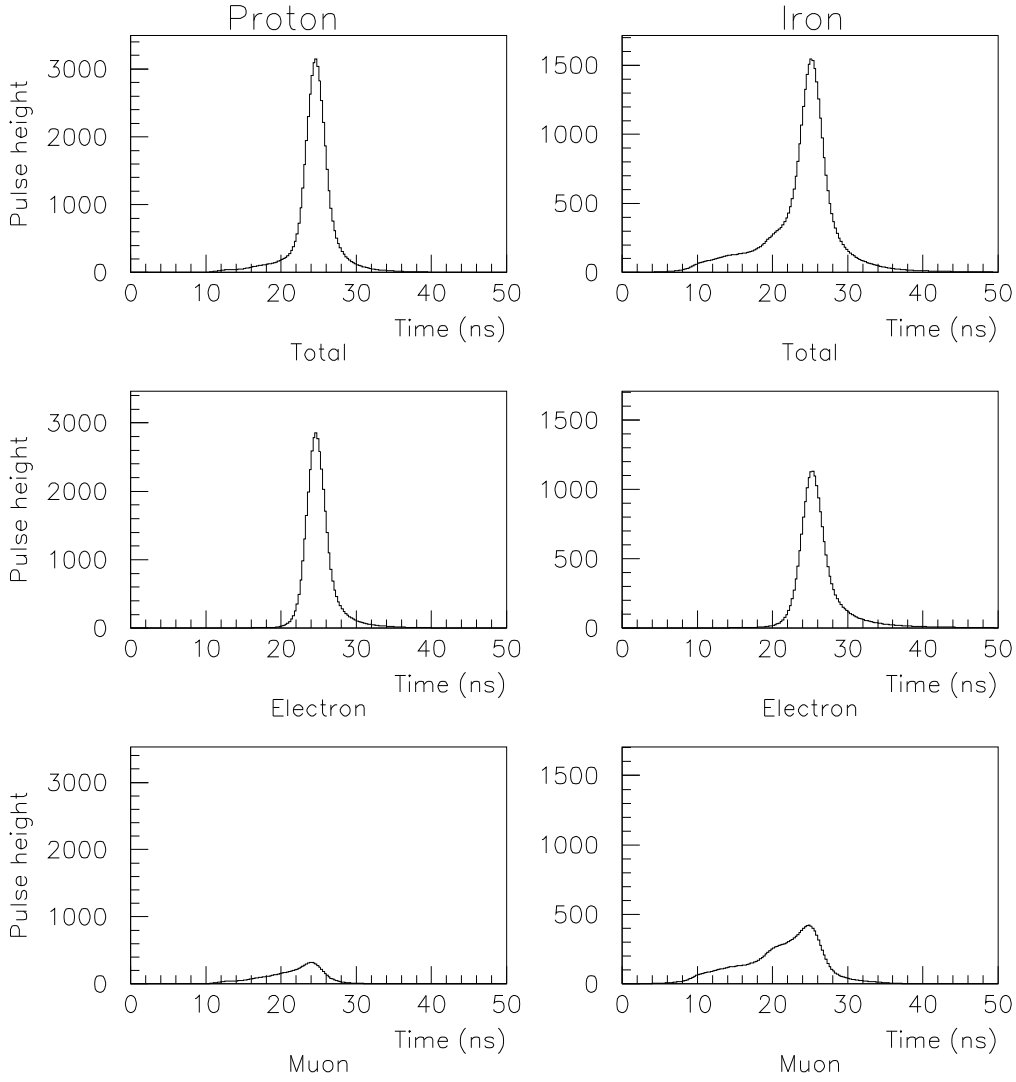

Fig. 3. Average Čerenkov pulse profiles for proton (left) and iron (right) primaries. The individual pulses have been aligned to minimize the chi-square differences between the Čerenkov light emitted by the electromagnetic component of each EAS. Also shown separately are the contributions to the average pulse profile from the muonic and electromagnetic components. The units of pulse height are arbitrary.

the interpretation of results. As the total atmospheric depth traversed by the Čerenkov light increases, the effects of atmospheric absorption become more important; this issue will be addressed in more detail in section 7.

Fig. 3 shows the average pulse profiles for proton and iron primaries at 60° from zenith. The pulses contain between 600 and 900 photoelectrons, but no other selection conditions have been applied. The pulse size selection acts to limit the range of energies (and subsequently core locations) that are present in the sample. The individual contributions to the Čerenkov pulse by the muonic and EM components are also shown. It can be seen that the muonic

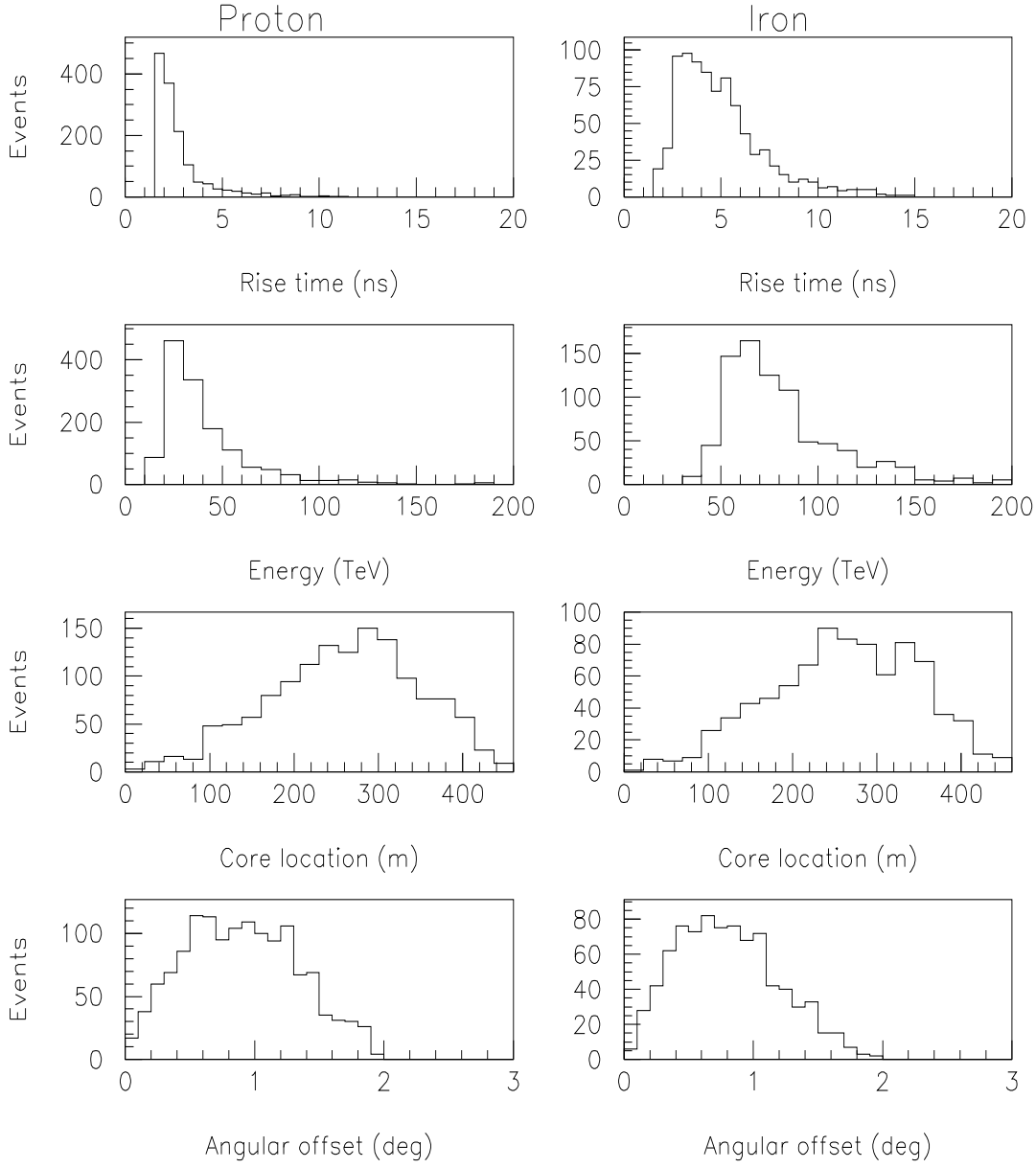

Fig. 4. Distributions of a number of different pulse and primary parameters for proton and iron primaries at 60° from zenith. The "Angular Offset" describes the arrival direction of the primary with respect to the center of the FOV. The selection criteria, described in detail in the text, applied to these samples are: 600 < photoelectrons < 900, FWHM < 5.0ns, LT-ratio > 0.1.

Čerenkov light is typically well in advance of the light from the EM component and that the muonic/EM Čerenkov light ratio of iron primaries is higher than that of proton primaries.

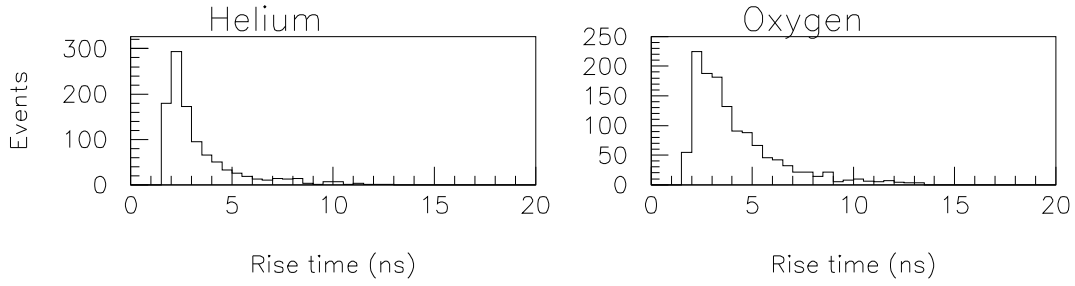

Fig. 5. The distribution of the Čerenkov pulse rise-time parameter for helium and oxygen primaries. The selection criteria used here are the same as those described in Fig. 4.

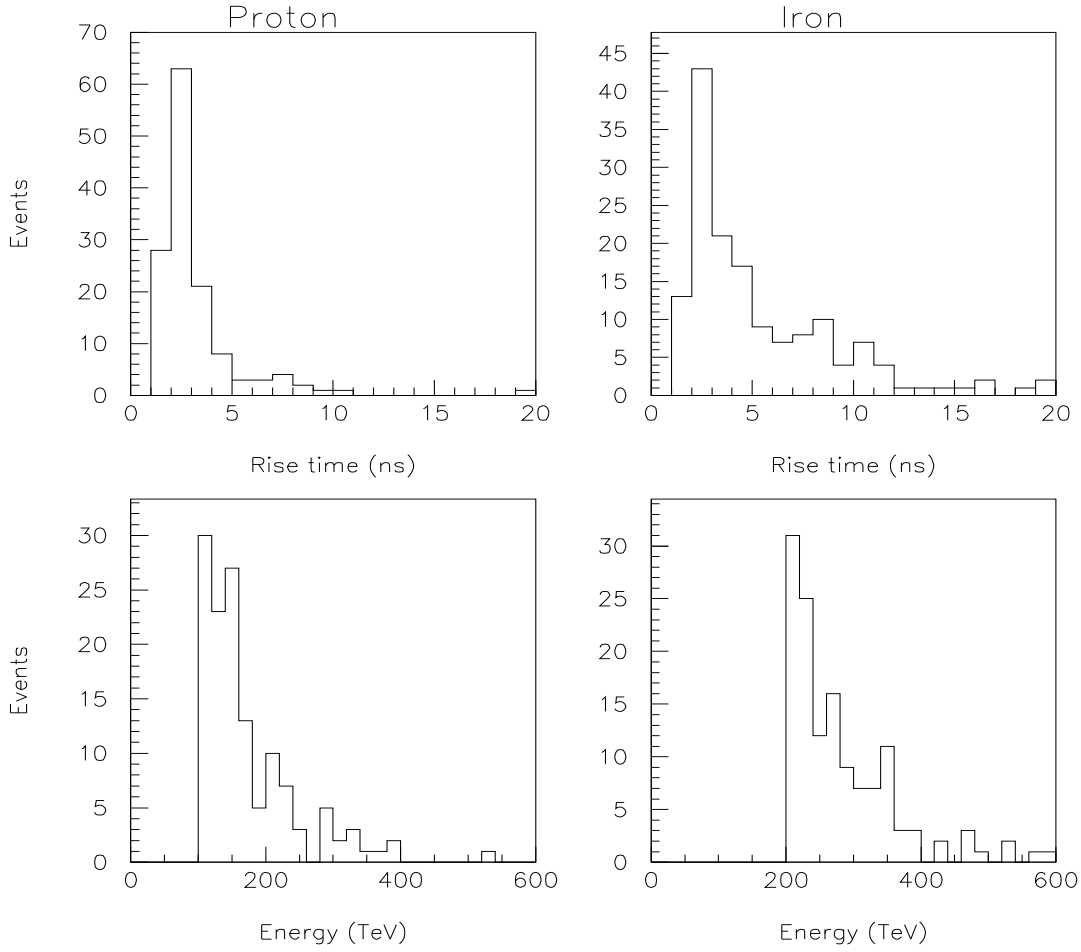

Fig. 6. The Čerenkov pulse rise-time and primary particle energy distributions of proton (left) and iron (right) induced EAS at 70° from zenith. Selection conditions: 600 < photoelectrons < 900; FWHM < 6.0ns, LT-ratio > 0.1.

The differences between iron and proton initiated Čerenkov pulse profiles can be seen in simple pulse parameters, such as rise-time (10% to 90% of pulse maximum) and full width at half maximum (FWHM). The distributions of these parameters as a function of core location are shown in Fig. 1 and Fig. 2. In addition to rise-time and FWHM a third parameter, called LT-ratio (Leading to Trailing signal ratio), will also be defined. The LT-ratio parameter is the ratio of the signal on the leading edge of the pulse to the signal on the trailing edge of the pulse. The signal on the leading and trailing edges are calculated from the sum of photoelectrons arriving in a 10ns period that starts 2.5ns and finishes 12.5ns from the maximum height of the pulse. The LT-ratio parameter is useful for rejecting a small number of events ($\sim$10% of iron and $\sim$5% of protons) where a large muon peak is present on the leading edge of the pulse. This peak can cause a mis-characterization of the pulse by the simplistic determination of the rise-time and FWHM parameters.

The relationship between primary composition and rise-time is strongest around the Čerenkov shoulder. The distribution of core locations can be limited to some extent by making a simple FWHM cut (see Fig. 1). Fig. 4 shows the distribution of rise-times and other parameters for proton and iron primaries after pulses with FWHM greater than 5.0ns have been rejected. There are clear differences between the Čerenkov pulse profiles of proton and iron initiated EAS and this is reflected in the distributions of the rise-time parameter. Also shown are the rise-time distributions of helium and oxygen primaries at 60° from zenith (Fig. 5), and of proton and iron primaries at 70° from zenith (Fig. 6).

Many of the difficulties in interpreting EAS data at ground level are due to the fluctuations in shower development. In particular, the depth of first interaction (DOFI) variation for primary protons causes large variations in the secondary particle properties at ground level. Fig. 7 shows that the Čerenkov pulse profile of a primary proton is largely independent of the DOFI.

6 Composition estimation

While clear differences exist between the pulse parameters of various primary species, the interpretation of experimental results leading to a composition estimate over a range of energies will clearly be complex. Even for a narrow range of total pulse sizes at a fixed zenith angle each primary species will have a different distribution of energies, core locations and arrival directions. As with other ground based experiments, correct interpretation of results will rely on accurate modeling of cascade development, atmospheric attenuation and the detector response.

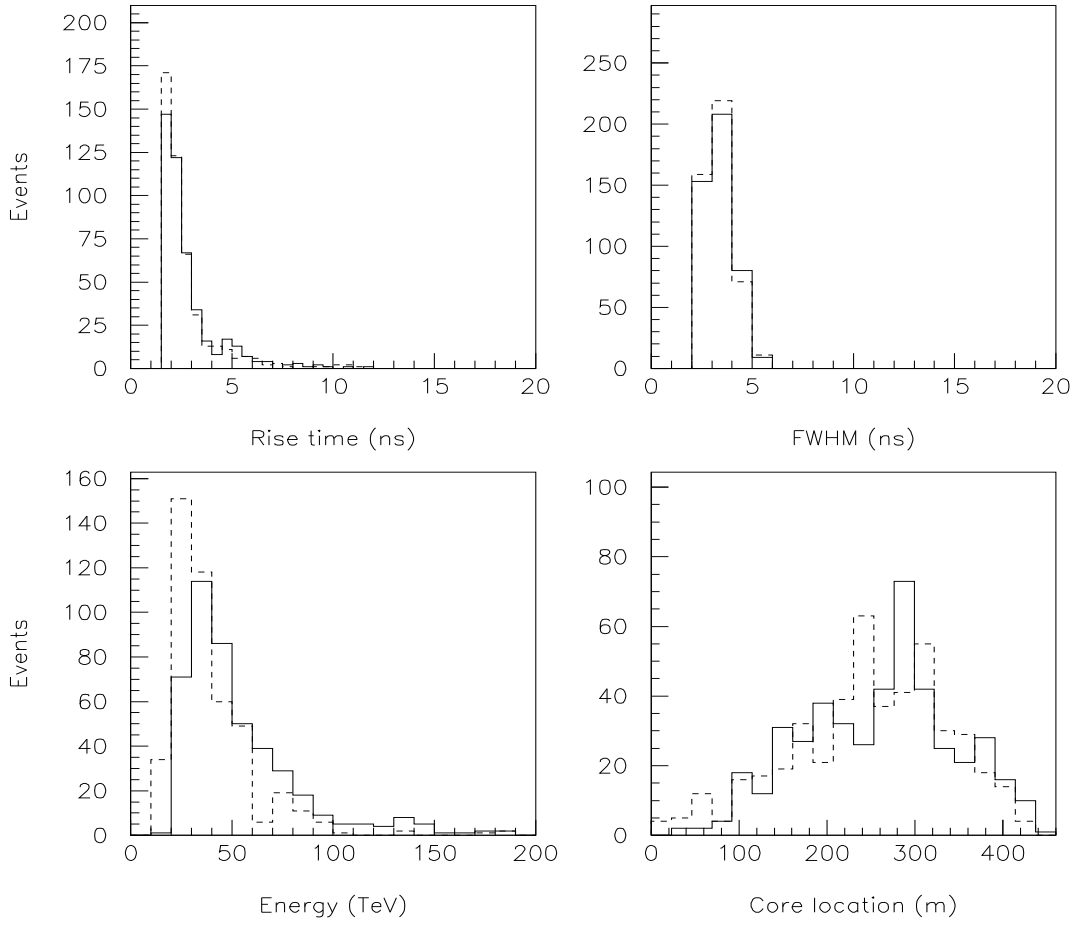

Fig. 7. The dependence, for protons primaries at 60° from zenith, of various pulse and primary parameters on the depth of first interaction (DOFI). The solid line is for proton initiated EAS with a DOFI less than 80 gcm^{-2}, the dashed line for DOFI greater than 80 gcm^{-2}. Selection conditions are those applied in Fig. 4.

The considerable overlap between the rise-time distributions of the various primary species shows that it will be impossible to assign unambiguously primary mass on an event by event basis. Instead, the composition may be inferred by combining the simulated rise-time distributions of individual primary species to reproduce the experimentally observed rise-time distribution. The Monte Carlo simulations allow the ratio of each species derived from such a comparison to be converted directly to a flux. If observations are taken over a range of zenith angles, such that the average energy at each zenith angle increases by a factor of say, 5, the energy spectrum for each primary species can be inferred over a wide range of energies. The assumed spectral index for each species within each energy band can be adjusted by statistical resampling, and the comparison process repeated to achieve consistency between the different

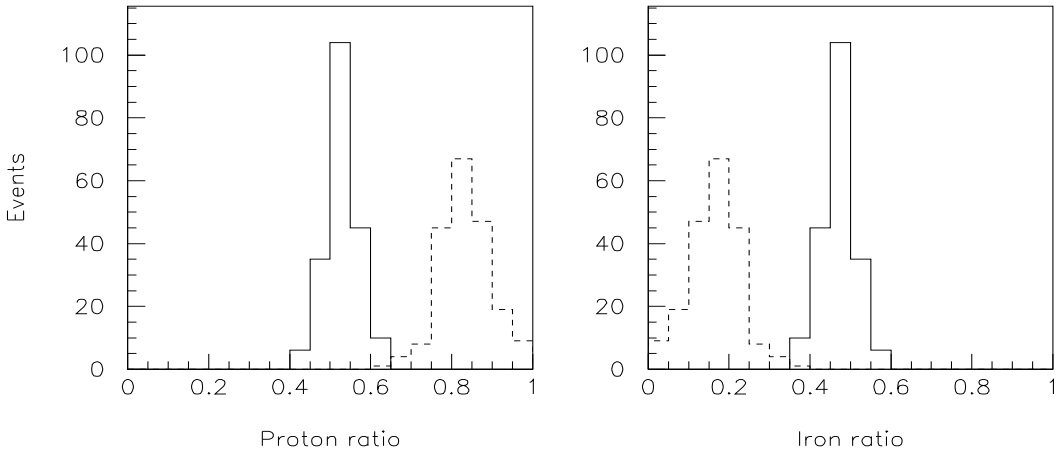

Fig. 8. The distribution in the predicted flux ratios of the primary species for actual flux ratios of (proton:iron=0.5:0.5) (solid lines) and (proton:iron=0.8:0.2) (dashed lines) (see the text for details).

energy bands.

An example of the accuracy to which the ratios of various primary species can be estimated is shown in Fig. 8. This example, at 60° from zenith, represents the simplest case, where the cosmic ray flux is assumed to consist of only protons and iron nuclei. The Monte Carlo data set for each species has been divided randomly into two halves. From the first half, a "test distribution" of rise-times has been created, which will represent an experimentally measured sample. If the test distribution is created assuming equal fluxes of proton and iron primaries, after allowing for triggering efficiency, collecting area and event selection, the ratios of events in the sample are (proton:iron=0.79:0.21). The second half of the Monte Carlo rise-time data set has then been repeatedly sampled, allowing the flux ratios of the primary species to vary over all possible values. Each of these "sample distributions" is then compared to the "test distribution" using a Kolmogorov-Smirnov (K-S) test. If the K-S test statistic indicates a probability greater than 90% that the test and sample distributions are drawn from the same parent distribution, then the primary ratios are recorded. The most probable ratio for each species is determined with high precision, but the absolute accuracy is limited - mainly by statistical fluctuations in the test distribution. Fig. 8 shows the distribution of most likely ratios of primary species for repeated regeneration of the test distribution. It should be noted that each test and sample distribution is not fully independent, each being drawn from a limited Monte Carlo data set. Each sampled distribution corresponds to only $\sim$ 10 hours of actual observations (400 events in each of the test and sample distributions). A reasonable observational data-set of several hundreds of hours duration, and more Monte Carlo simulations, would provide greater flux accuracy than indicated in Fig. 8.

The procedure described above can also be applied to a four component cosmic ray flux (proton:helium:oxygen:iron), although the flux accuracy is reduced compared to the two component (proton and iron) fit. In addition, with the limited size of the Monte Carlo data set, a completely unbiased search is not possible, and the range of compositions searched must be limited to avoid local statistical minimums in the differences between the test and sample distributions.

7 Experimental considerations

One of the advantages of using a single mirror/single PMT combination is the ease of calibration of such an experiment. The mirror reflectivity, PMT quantum efficiency, gain and impulse response can all be accurately determined. The background noise to the Čerenkov pulses can be easily monitored and incorporated into Monte Carlo simulations. The greatest source of uncertainty will be in characterizing the atmosphere, and in particular describing the absorption of the Čerenkov light in the atmosphere. Failure to correctly describe the absorption profile of the atmosphere will distort the apparent ratio of light emitted at varying depths from the observation point.

Demanding consistency of pulse parameter distributions on a night by night basis should reject nights where the atmosphere is disturbed (significantly different from a molecular atmosphere). In addition to this, atmospheric attenuation could be measured directly through stellar extinction and ground-level standard light sources placed at varying distances from the observatory. Although accurate accounting for absorption is most critical for observations at large zenith, the effects should also be observable for near-zenith observations. It should be possible, therefore, to gauge the accuracy of the absorption estimate and other calibration procedures by comparing the Čerenkov pulse profile estimate of the primary cosmic ray composition with that obtained by direct measurement. This comparison should also be useful in determining the accuracy of the Monte Carlo simulations as a whole.

8 Conclusion

Monte Carlo simulations presented in this paper have shown that the temporal distribution of Čerenkov light emitted from EAS is sensitive to the muon/electron ratio of the cascade. Using a single large area mirror coupled to a narrow field of view photo-detector, it is possible to use these pulse profiles to estimate the chemical composition of primary cosmic rays over a large range of energies.

Acknowledgement

The author would like to thank Philip Edwards, Jamie Holder, Bruce Dawson John Patterson, Roger Clay and Gavin Rowell for helpful comments. The author acknowledges the receipt of a JSPS postdoctoral fellowship.

References

[1] V.R. Chitnis, P.N. Bhat, *Astropart. Phys.* (1999) in press

[2] J.E. Dickinson et al., 25^{th} *ICRC, Durban* **5** (1997) 229

[3] M. Hess et al., *Astropart. Phys.* (1999) in press

[4] A.M. Hillas, *J. Phys. G:Nucl. Phys.* **8** (1982) 1475

[5] H.O. Klages et al., *Nucl. Phys. B (Proc. Suppl.)* **52B** (1997) 92

[6] J. Knapp, D. Heck, Extensive Air Shower simulation with CORSIKA, v4.5: A user's guide

[7] A. Lindner, *Astropart. Phys.* **8** (1998) 235

[8] L.F. Fortson et al., 25^{th} *ICRC, Durban* **4** (1997) 49

[9] J.R. Patterson, A.M. Hillas, *J. Phys. G:Nucl. Phys.* **9** (1983) 1433

[10] M.D. Roberts et al., *J. Phys. G:Nucl. Phys.* **24** (1998) 255

[11] A.A. Watson, 25^{th} *ICRC, Durban* **8** (1997) 257

[12] J. Wdowczyk, *J. Phys. G:Nucl. Phys.* **20** (1994) 1001